World Journal of Advanced Engineering Technology and Sciences
eISSN: 2582-8266
Cross Ref DOI: 10.30574/wjaets
Journal homepage: https://wjaets.com/

(RESEARCH ARTICLE)

Check for updates

Aeromagnetic investigation of crustal stability of Osi, north central Nigeria

Olafisoye Emmanuel Rotimi *, Olaniyan Isaac Oladejo and Fakorede Solomon Oguns

Department of Physical Sciences, Olusegun Agagu University of Science and Technology, Okitipupa, Ondo State, Nigeria.

World Journal of Advanced Engineering Technology and Sciences, 2022, 05(02), 136–151

Publication history: Received on 14 March 2022; revised on 22 April 2022; accepted on 24 April 2022

Article DOI: https://doi.org/10.30574/wjaets.2022.5.2.0053

Abstract

High-resolution aeromagnetic data of Osi north central Nigeria has been processed with a view to establish the earthquake-prone fault zones in the area. The analytical signal amplitude, shaded relief total horizontal derivative, first vertical derivative and 3D Euler deconvolution maps produced from the residual magnetic intensity anomalies of the study area identified the structural features in the area. The locations and the orientations of the extracted magnetic lineaments were revealed by the structural map of the area and the associated rose diagram. The lineaments were observed to strike NE-SW, ENE-WSW, E-W, NW-SE, WNW-ESE, NNE-SSW and NNW-SSE. The upward continuation maps showed evidence of deep-lying faults while the source parameter imaging and spectral analysis revealed depth to magnetic sources ranging from 81 m to 402 m and 103 m to 460 m respectively. The predominant NE-SW and NNE-SSW trending faults in the study area depicted stress history related to Ifewara faults; which is an indication of possible impending earthquake occurrence in the area.

Keywords: Ifewara; Osi; Fault Zone; Earthquake; Magnetic Basement; Total Horizontal Derivative

1. Introduction

The world's most prominent fault zones are found in United State of America, Mexico, Colombia, Venezuela, Chile, Japan, Indonesia, Fiji and Tonga; with records of major tectonic events. The earthquake measured in these regions ranged from 7.7 to 9.5 in magnitude on the Richter's scale. Recently, in Africa, there have also been pockets of seismic activities in Djibouti, Eritrea, Ethiopia, Kenya, Somalia and Nigeria; where minor earthquakes with magnitude less than 5.9 were recorded. Studies have revealed that the drifting apart of the South American and African plates created the South Atlantic Ocean approximately 145 million years ago [1]; where chains of seismic events have been experienced till date.

The St. Paul Fracture Zone and the Romanche trench resulting from the opening of the South Atlantic Ocean traversed perpendicularly to the mid-ocean ridge into the Nigeria landmass [2]; producing a weak zone of tectonic instability within the region. In Nigeria, the National Space Agency has identified areas in some states prone to seismic hazards. These areas which are likely to be epicenters of major earthquakes in the country include: Mpape in Federal Capital Territory, Kwoi in Kaduna state, Ijebu Ode in Ogun state, Shaki in Oyo state and Igbogene in Bayelsa state [3]. Earthquake-related studies conducted by notable researchers have revealed that tremor recorded in the aforementioned locations might be connected to the Ifewara-Zungeru fault zone; extending from the northwestern to the southwestern region of Nigeria. These recurring tremors are suspected to have originated from the South Atlantic Ocean [4], and could be a buildup to a major earthquake [5].

The NNE-SSW trending Ifewara fault plane stretches across a distance of approximately 250 km, and extends from the eastern part of Ijebu ode, southwestern Nigeria to the southwestern section of river Niger within the Nupe basin [5], where it links with the NNE-SSW trending Zungeru fault at the northeastern flank of the basin. The Ifewara and Zungeru

* Corresponding author: Olafisoye Emmanuel Rotimi
Department of Physical Sciences, Olusegun Agagu University of Science and Technology, Okitipupa, Ondo State, Nigeria.

transcurrent faults occur within the Precambrian basement complex of Nigeria and have been linked to the Atlantic Fracture System [4-6]; which is a linear discontinuity in the oceanic crust. The Ifewara fault zone is composed of meta-supracrustal and migmatitic gneiss sequence [4] and traverses the Okemesi fold belt. This fault zone is geologically underlain by amphibolites, amphibolite schists, quartz schists, with associated pegmatites and gneisses at the western regime, while on the eastern section, rocks consist mainly of quartzites and quartz schists with associated quartzofeldspathic gneisses.

Studies further revealed that the Ifewara fault is a shear zone of flat-lying mylonites, with characteristic contractional tectonics [7] similar to the Zungeru fault [8]. Several tremors that have emanated from this fault zone have resulted to building damages and loss of property in residential areas that are within close proximity. Hence, the destructive and hazardous effects of deep-lying geologic structures necessitated the need for this study.

2. Geological Setting

The geology of the study area falls within the north central Nigerian Basement Complex as shown in Figure 1; comprising the Migmatite-Gneiss Complex, the Schist Belt (metasedimentary and metavolcanic rocks), and the Older Granites (Pan-African granitoids) [9]. The Migmatite-Gneiss Complex ranged from Pan-African to Eburnean age [10-11]. The schist belts are made up of low-grade metasediment-dominated belts which are fault-controlled rift-like structures [12]. This forms the Upper Proterozoic supracrustal rocks that have been infolded into the migmatite-gneiss-quartzite complex. The Older Granites which consist of granite gneiss, hornblende granite, medium/coarse-grained biotite granite, granodiorite and porphyritic granite; are the most obvious manifestation of the Pan-African orogeny and occur intricately associated with the Migmatite-Gneiss Complex and the schist belts into which they generally intruded [9].

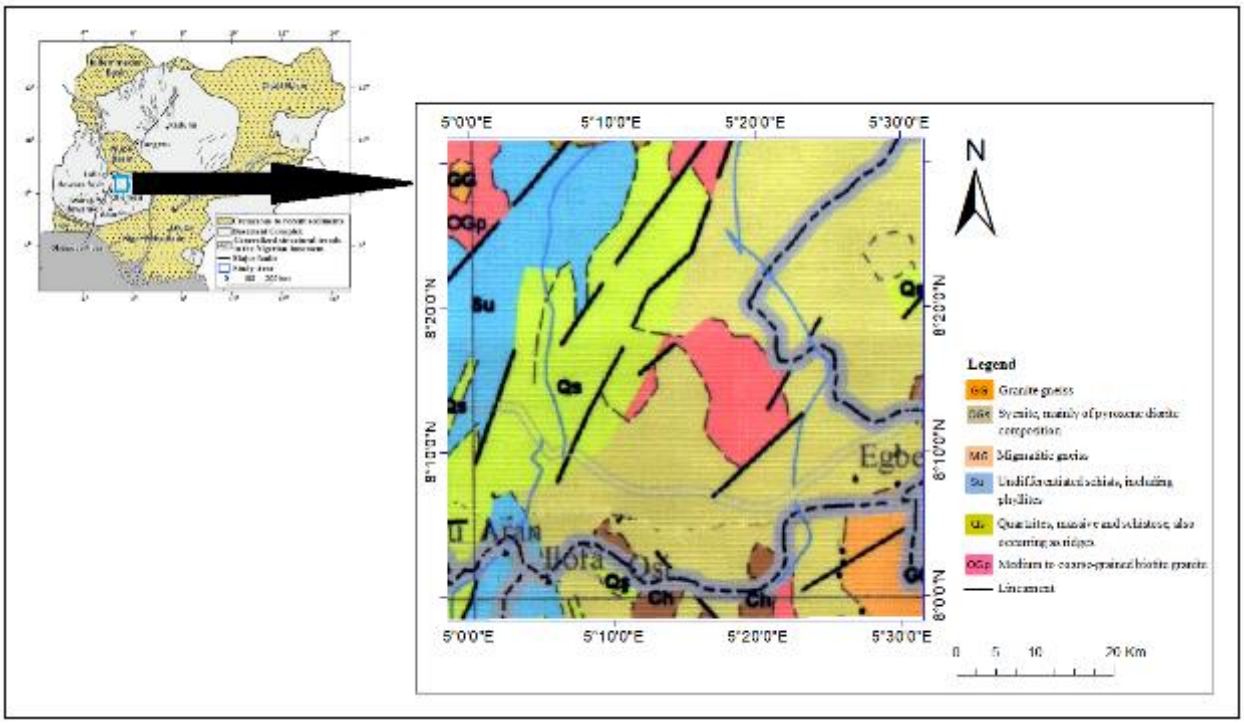

Figure 1 Geological map of Nigeria showing the study area

3. Material and methods

3.1. Aeromagnetic data analysis

High-resolution aeromagnetic data (HRAD) bounded by latitudes 8.00° to 8.30° N and longitudes 5.00° to 5.30° E used for this study was acquired from Nigeria Geological Survey Agency (NGSA). The acquired data was gridded at 100 m spacing using the minimum curvature gridding method to produce the total magnetic intensity (TMI) map of the study

area. The data was measured at intervals of approximately 7 m with a nominal flight height of 80 m above the terrain. A flight line spacing of 500 m and tie line spacing of 2 km was adopted in the survey with flight line in the NW–SE direction while the tie lines trend in the NE–SW direction. The high-resolution aeromagnetic data were processed using geosoft oasis montaj, surfer ™ version 12 and georose software applications.

The total magnetic intensity map of the study area was subjected to reduction-to-equator technique for accurate positioning of the various anomalies over their corresponding magnetic sources. This study applied reduced-to-equator approach because it is suitable for low latitude areas and helps to simplify interpretation by transforming magnetic data recorded at various magnetic field inclinations to zero inducing field inclination [5]. The reduction-to-equator map was upward continued to 200 m to remove cultural noise (high frequency signals) from sources on or near the ground surface. The resulting map was further filtered by the removal of regional field; corresponding to an upward continued height of 80 km. The residual magnetic intensity map was then obtained after the regional field removal.

Source edge detection methods were then applied to the residual magnetic intensity map to enhance the subsurface geological structures and lithological boundaries associated with fractures, faults and contacts in the study area. These methods include: upward continuation, first vertical derivative, analytic signal magnitude, total horizontal derivative and Euler Deconvolution.

Upward continuation method transforms magnetic data to that which would be observed at different depths below the actual observation level. This filtering method suppresses high frequency anomalies, thereby attenuating the effect of near surface magnetic sources relative to deeper sources. It can be expressed mathematically as:

$$L(r) = e^{-hr}, \tag{1}$$

The expression for r is given as

$$r = \sqrt{u^2 + v^2} = 2\pi k. \tag{2}$$

where h is the new height, u and v are the wave numbers in the Fourier domain and k is cycles/unit.

The first vertical derivative filtering method enhances the short wavelength responses in the data by suppressing the long wavelength anomalies. It is applied because it is the least susceptible to noise when compared with the higher order vertical derivatives.

Analytic Signal Magnitude (ASM) can be expressed as the square root of the squared sum of the vertical and horizontal derivatives of the magnetic field [14].

$$ASM = \sqrt{\left(\frac{\partial M}{\partial x}\right)^2 + \left(\frac{\partial M}{\partial y}\right)^2 + \left(\frac{\partial M}{\partial z}\right)^2}. \tag{3}$$

Analytic signal method does not depend on the direction of magnetization [15], but peaks over the edges of source bodies. This magnetic data enhancement method can also be used to depict the source edge locations.

Total horizontal derivative (THDR) method is extensively used to estimate boundaries of shallow magnetic bodies. This filtering technique which shows low sensitivity to noise has high amplitude over the edge of the magnetic sources. The total horizontal derivative can be determined by the equation below:

$$THDR = \sqrt{\left(\frac{\partial M}{\partial x}\right)^2 + \left(\frac{\partial M}{\partial y}\right)^2}. \tag{4}$$

Where $\frac{\partial M}{\partial x}$ and $\frac{\partial M}{\partial y}$ are the two horizontal derivatives of the observed field (M).

Euler Deconvolution was also employed for the delineation of magnetic source geometry, location and depth. It is, therefore, a boundary finder and depth estimation method. Assuming (x_o, y_o, z_o) is the position of a magnetic source and the total field (M) measured at a point (x, y, z) has a regional value of B, the Euler's homogeneity equation as defined by Reid et al. [16] will be

$$(x - x_o)\frac{\partial M}{\partial x} \rightarrow +(y - y_o)\frac{\partial M}{\partial y} + (z - z_o)\frac{\partial M}{\partial z} = N(B - M). \quad (5)$$

where N is the structural index value chosen based on the magnetic source geometry. N can be denoted as 0, 1, 2, or 3 for contact, sill/dike/fault, pipe/horizontal or sphere, respectively.

Thompson [17] and Reid et al. [16] suggested that a correct N gives the tightest clustering of the Euler solutions around the geologic structure of interest.

Spectral analysis was also employed for the estimation of depth to magnetic sources through the application of Fast Fourier Transform approach. It is a function of wavelengths in both the x and y directions. The windowed grid is processed to become periodic at its edges. The Fourier transform f(μ,γ) of periodic function f(x,y) is given by Lee [18] as:

$$f(\mu\gamma) = \int_{-\infty}^{+\infty}\int_{-\infty}^{+\infty} f(x,y)\cdot e^{-i(\mu x+\gamma y)}dx\cdot dy. \quad (6)$$

where (x) and (y) are the spatial coordinates in the x and y directions respectively.

μ and γ are the angular frequencies in the x and y directions respectively.

The source parameter imaging [19-20] or the local wavenumber method [21] is based on the principle of complex analytic signal which computes source parameters from gridded magnetic data. This method requires computation of the first- and second order derivatives, making it susceptible to noise and interference effects [22]. Hence, for vertical contacts, the peaks of the local wavenumber define the inverse of depth. The depth can therefore be calculated using the formula:

$$\text{Depth} = \frac{1}{K_{max}}, \quad (7)$$

Where K_{max} is the peak value of the local wavenumber K over the steep source. Hence, the wavenumber is given by the expression:

$$K_{max} = \sqrt{\left(\frac{\partial \text{Tilt}}{\partial x}\right)^2 + \left(\frac{\partial \text{Tilt}}{\partial y}\right)^2}. \quad (8)$$

In this study, the depth estimation methods were used to determine the depth to anomalous causative bodies and to map the basement topography.

4. Results and discussion

4.1 Total magnetic intensity map

The total magnetic intensity map (Figure 2) produced from high-resolution aeromagnetic data sheet of Osi revealed variations in the magnetic field intensity of the study area. This is attributed to the presence of different magnetic rocks with different mineral contents existing at varying depths at the subsurface. The amplitude of the magnetic field intensity ranged from -22 to 120 nT showing linear discontinuities of anomalies trending predominantly in the northeast-southwest direction. The short wavelength anomalies depicted in the area correspond to near-surface magnetic outcrops while long wavelength revealed deep-seated basement rocks.

Figure 3 represents profiles which depict the relationship between the residual, reduced to equator and total magnetic intensity anomalies beneath the study area. The profiles that extend from west to east across Osi area further establish the trend and the variation in the magnetic intensity signatures.

4.2 Reduction to Equator Map

Reduction to equator (RTE) filtering was performed on the total magnetic intensity data with inclination and declination values of 8.41° and -1.4° respectively. The amplitudes of the magnetic anomalies ranged between -18 and 115 nT in the reduced to equator map (Figure 4) which shows slight variation from the total magnetic intensity anomalies. The

resulting filtered map with anomalies better positioned above the causative bodies was subsequently upward continued to 200 m to attenuate high frequency responses associated with near-surface noise in the data.

4.3 Residual magnetic intensity and regional field maps

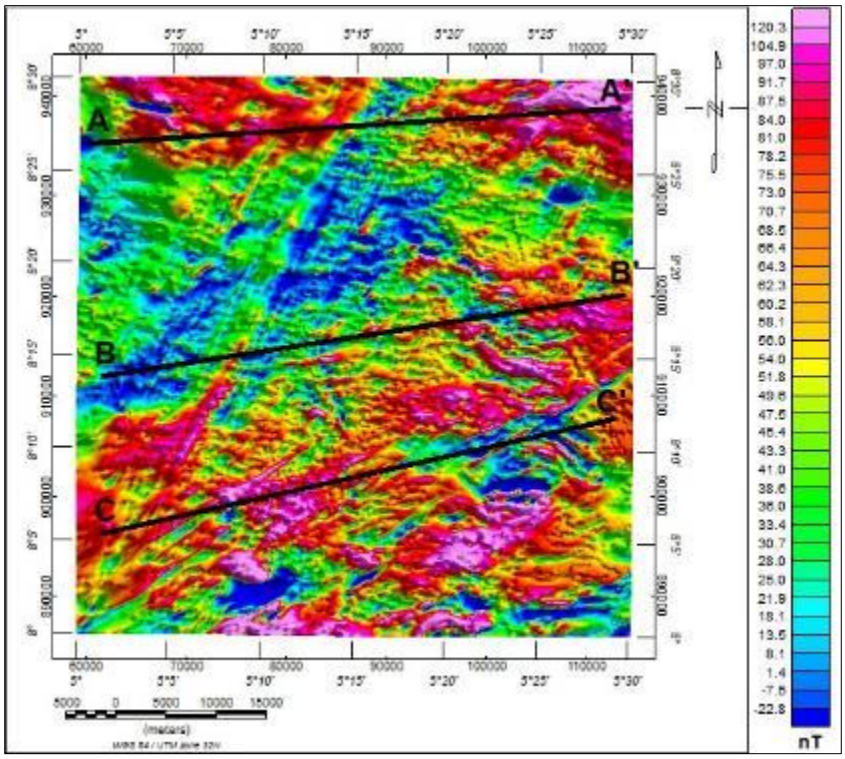

Figure 2 Total magnetic intensity map of the study area showing profiles A-A', B-B' and C-C'

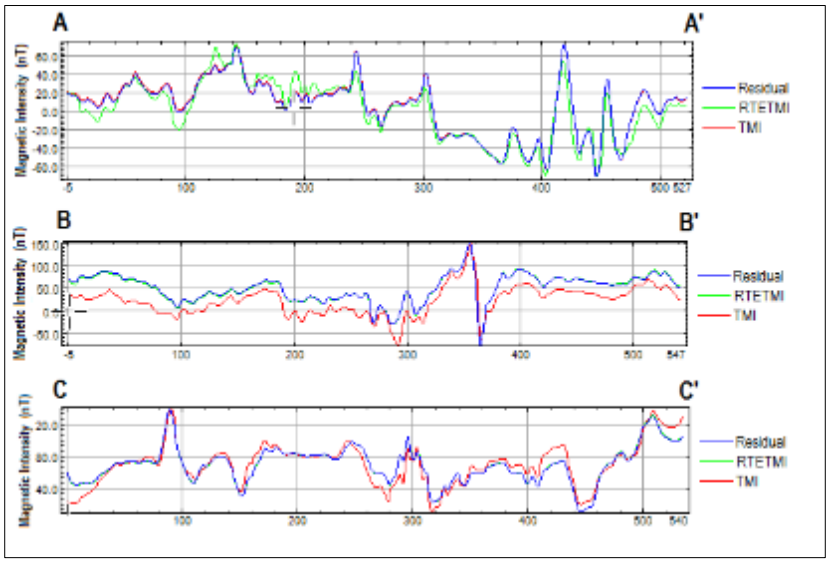

Figure 3 Magnetic intensity anomaly trend of residual, reduced to equator and total magnetic intensity along the profiles

The near-surface noise filtered map was upward continued to a depth of 80 km to produce the regional field map of the study area. This resulting field map was subsequently subtracted from the former to reveal the residual magnetic anomalies associated with tectonic events. The residual magnetic intensity map (Figure 5) showed linear anomalies

with varying magnetic susceptibility contrasts trending in the NE-SW direction within the study area similar to the total magnetic anomalies.

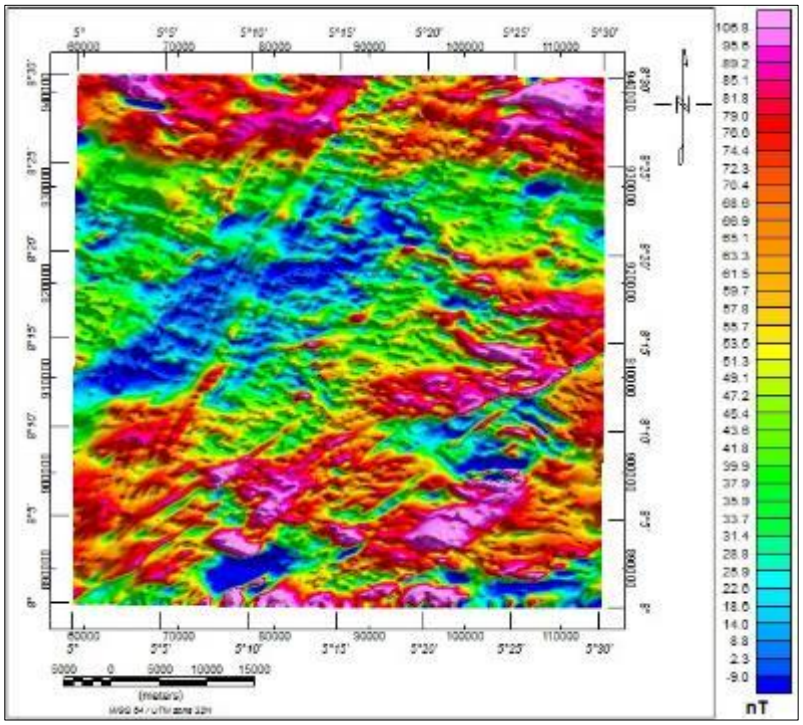

Figure 4 Reduced to equator map of the study area

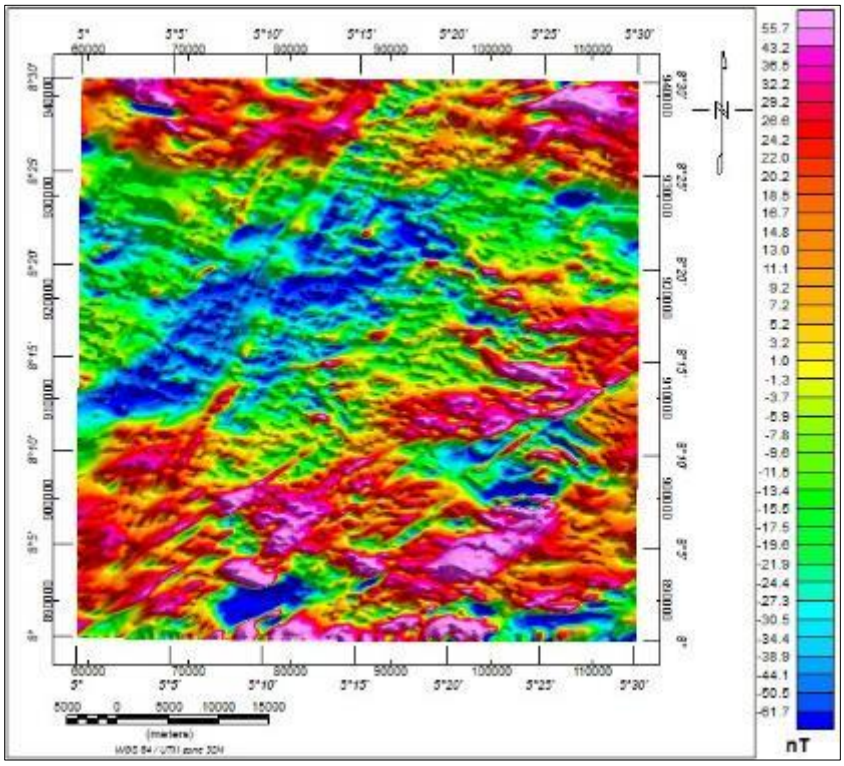

Figure 5 Residual magnetic intensity map of the study area

4.4 First vertical derivative

The First Vertical Derivative (FVD) was applied to the residual magnetic intensity map to accentuate source edge locations by suppressing the long wavelength anomalies (deep-lying magnetic features) in the study area. The resulting filtered map (Figure 6) reveals that short wavelength anomalies associated with shallow geological features are clearly emphasized within the study area. This is characteristic of basement complex rocks.

4.5 Analytic signal amplitude maps

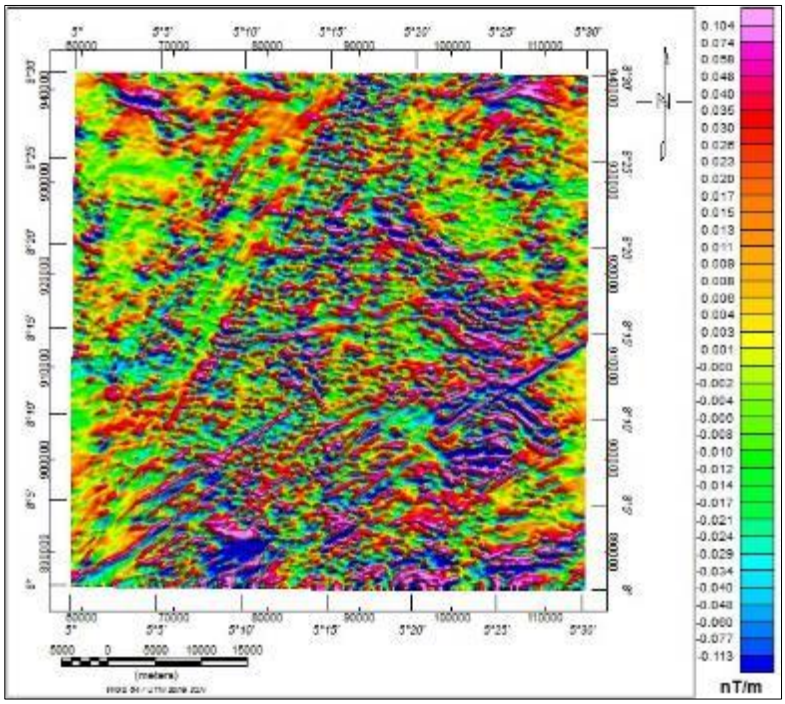

Figure 6 First vertical derivative map of the study area

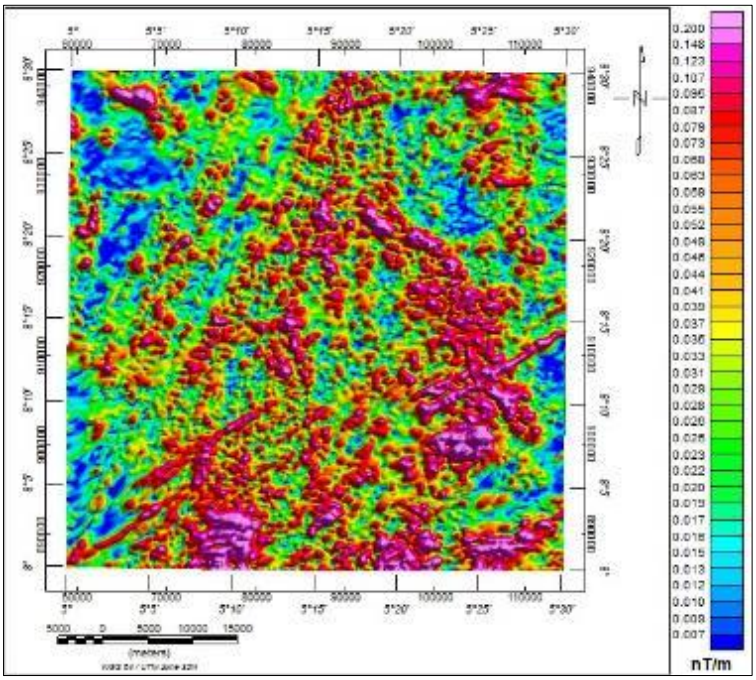

Figure 7 Analytic signal amplitude of the study area

The analytic signal amplitude map of the filtered RTE map is presented in Figure 7. The amplitude of analytic signal establishes contacts between magnetic bodies; revealing geologic structural complexity in the basement rocks. The maxima of the ASA map are continuous, thin, and straight peaking over the source edges in the study area as shown in Figure 8.

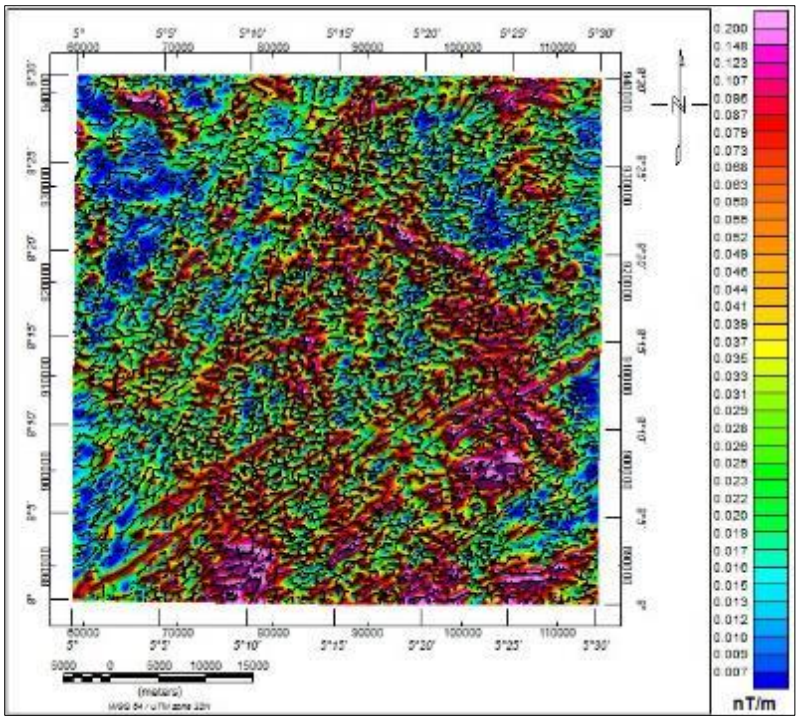

Figure 8 Maxima of analytic signal amplitude peaking over the lithological boundaries in the study area

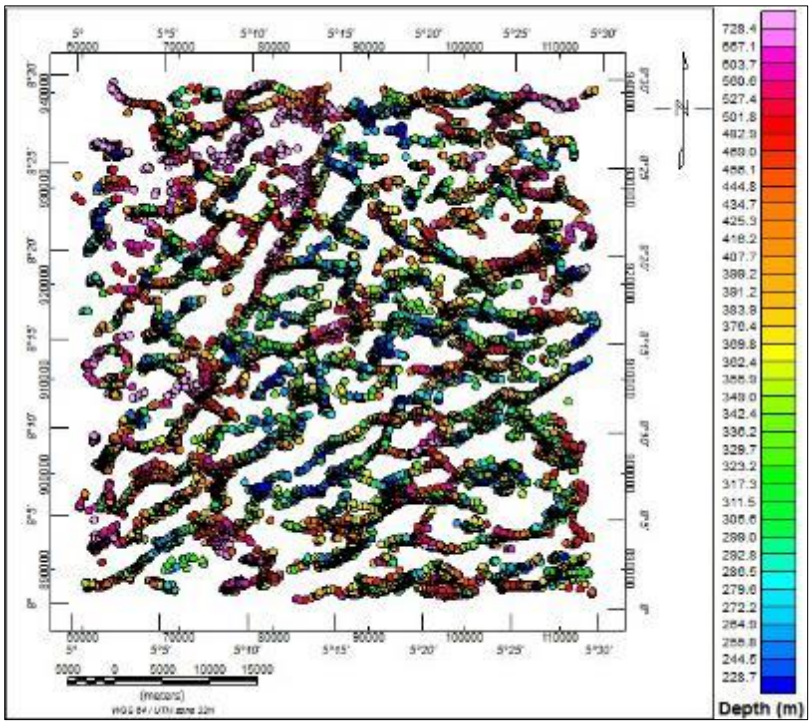

Figure 9 Plot of solutions of Euler deconvolution using structural index of 2

5 Depth estimation

5.1 Euler deconvolution

The plot of the 3D Euler Deconvolution of the study area is presented in Figure 9. The Euler solution obtained at structural index of two (2) gave the best clustering around some notable geologic features; linearly clustered solutions are interpreted as faults or lithological contacts; while oval-shaped clustered solutions are interpreted as intrusive bodies. The clustered Euler solutions were observed to depict the source edge locations also mapped by the first vertical derivative and analytic signal amplitude methods.

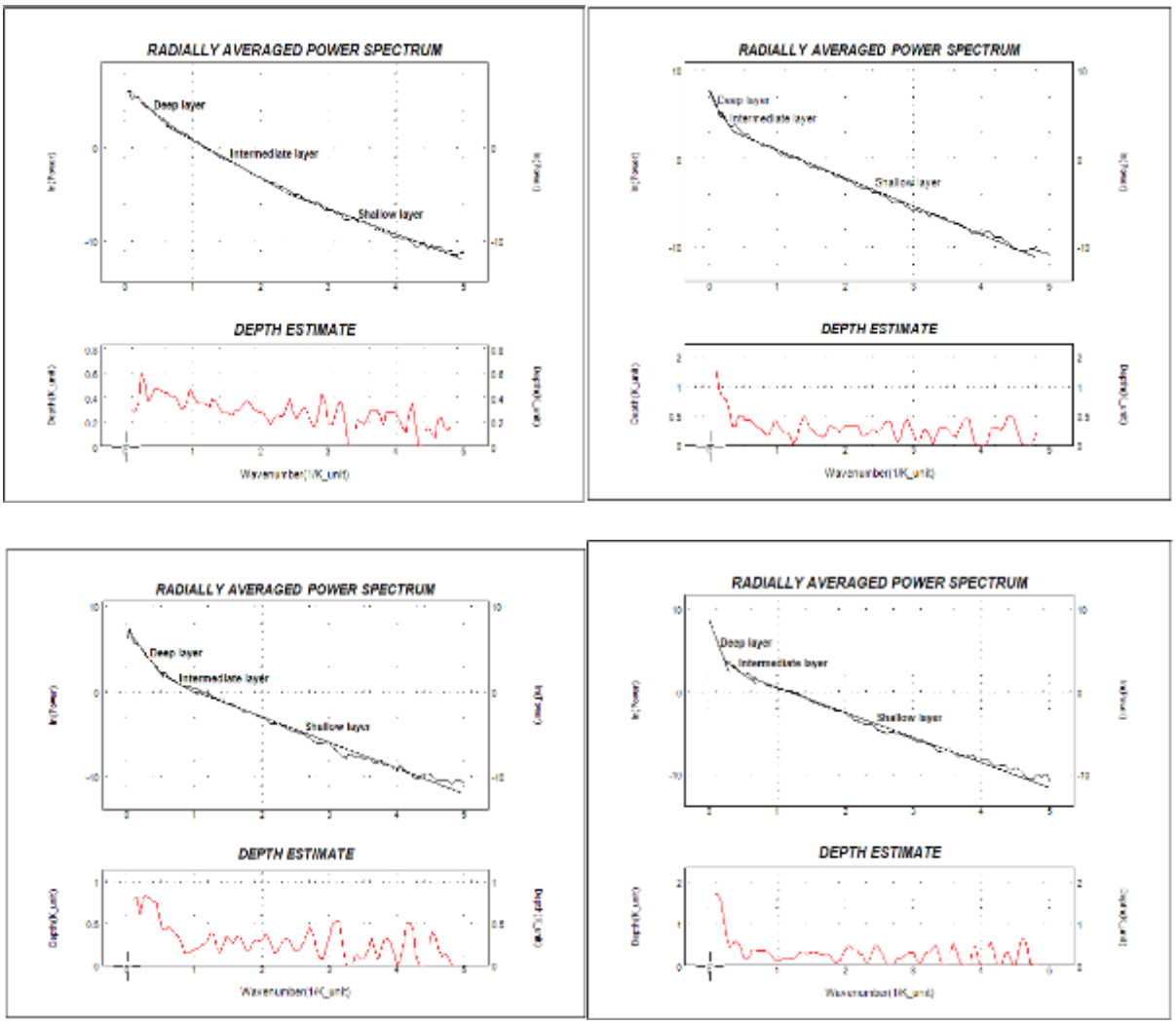

Figure 10 Radially averaged power spectrum estimate of depth to magnetic sources

5.2 Spectral analysis

Spectral analysis was also performed on the residual magnetic intensity map of the study area. Depth to magnetic sources was computed using the power spectrum method [23] which is a well-established tool for estimating the depths of magnetised bodies [24-27]. The depth estimated as shown in Figure 10 ranged between 103 m and 460 m and correlated well with the depth obtained from the Euler solutions (249 m to 748 m) and source parameter imaging methods (81 m to 402 m) for shallow and deep magnetic sources respectively.

5.3 Source parameter imaging

The source parameter imaging (SPI) map which reveals variations in the overburden thickness within the study area is presented in Figure 11. Shallow lying magnetic bodies are predominant in the study area, however, deep lying basement rocks are observed in the northwestern part of the area.

Table 1 Depth estimation from spectral analysis

Spectra Blocks	Eastings		Northings		Depth (km)		
	Xmin	Xmax	Ymin	Ymax	Shallow	Intermediate	Deep
1	59033.16	77653.89	925444.23	942090.04	0.01	0.02	0.04
2	77512.83	96133.56	925303.16	941948.97	0.04	0.16	0.34
3	95992.49	114613.22	925444.23	941666.84	0.02	0.06	0.07
4	59033.16	77653.89	905553.90	925585.30	0.05	0.08	0.4
5	77512.83	96133.56	905553.90	925585.30	0.03	0.03	0.08
6	95992.49	114613.22	905412.84	925585.30	0.05	0.08	0.3
7	58892.10	77653.89	886086.78	905694.97	0.02	0.05	0.1
8	77512.83	96133.56	885945.71	905553.90	0.03	0.05	0.2
9	95992.49	114472.16	885945.71	905694.97	0.02	0.04	0.12

The depth to basement in the study area ranged from 81 m to 404 m. However, in Figure 11, the observed depressions existing beyond 404 m depth on the profiles are suspected to be contacts/ faults locations.

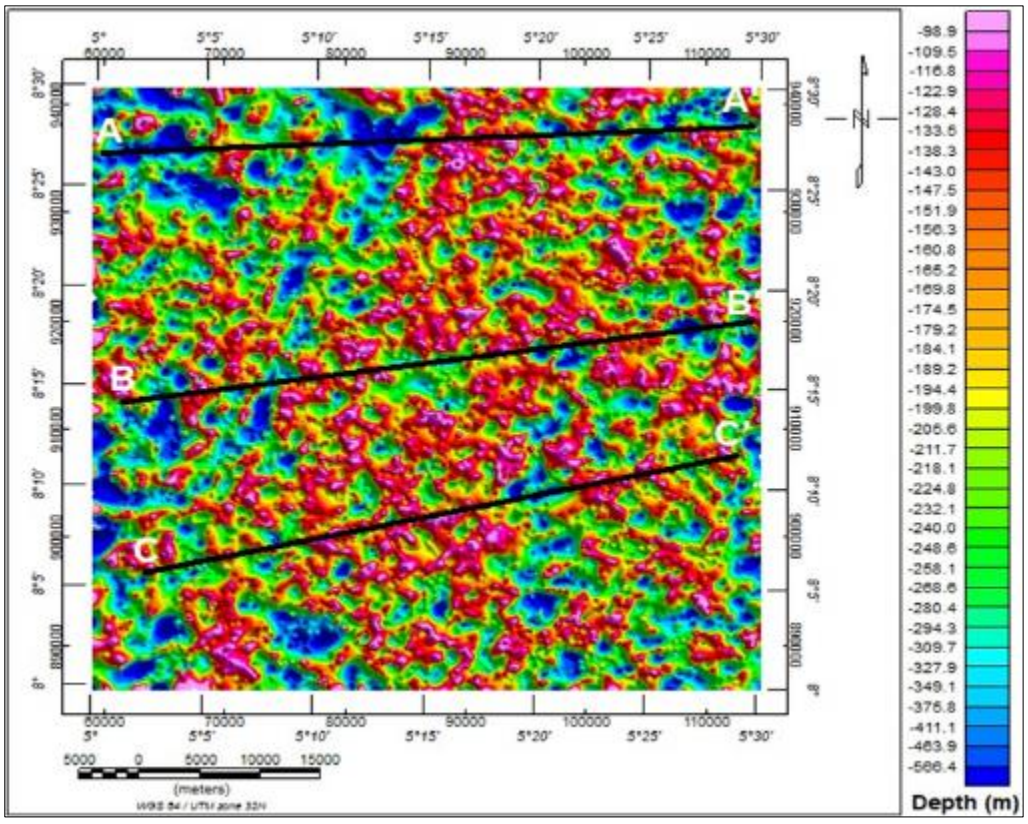

Figure 11 SPI map of the study area showing profiles A-A', B-B' and C-C'

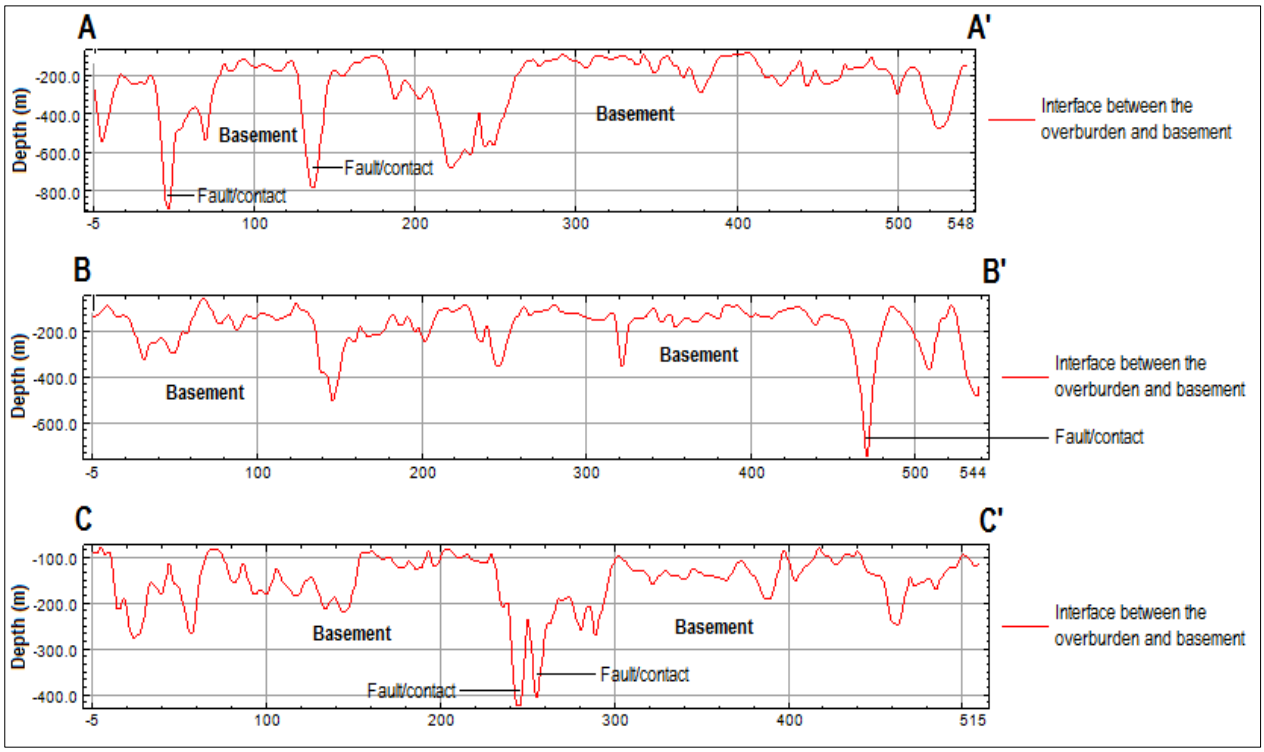

Figure 12 Overburden thicknesses along the Profiles

6 Structural map

6.1 Upward continuation maps

In the study area, geologic structures associated with faults were delineated from the upward continuation maps as presented in Figure 13. These filtered maps were produced from the transformation of the residual magnetic intensity anomalies to upward continued heights of 200 m, 700 m, 1500 m and 3000 m, respectively, above flight line elevation. The amplitude of the magnetic anomalies of the enclosed portions of the upward continuation maps was observed to decrease from a height of 200 m to 3000 m; indicative of faulted basement complex rocks at the subsurface within the study area.

6.2 Total horizontal derivative map

The total horizontal derivative map of the study area is presented in Figure 14. The gradients of the map ranged between 0.004 nT/m and 0.249 nT/m, and the amplitude peaks above the boundaries of magnetic structures related to lithological contacts in the study area.

The shaded relief total horizontal derivative map presented in Figure 15 was used to further delineate the structural features beneath the study area and the result was presented as the structural map of the area (Figure 16).

The extracted lineaments superimposed on the residual magnetic intensity map presented in Fig. 17 revealed that some lineaments are in concordance with the residual anomalies known as ductile deformation; while the rest are at discordant with the residual anomalies known as brittle deformation. Ductile deformations are associated with folds, whereas brittle deformations resulted in fractures and faults. Furthermore, a visual comparison of tectonic history of the major faults mapped in the study area with Ifewara faults revealed evidence of related crustal deformation trend. These faults were also observed to strike in the NE-SW direction similar to the Ifewara faults. The Rose diagram (Figure 18) was also produced and analyzed to depict the orientations of the extracted lineaments. The orientations revealed E-W, NE-SW, WWN-EES, N-S, WWS-EEN and SSW-NNE trends as shown in Figures 17 and 18; which is an indication of complexity in structural geology of the study area. The northeast-southeast alignment is associated with Pan African orogeny, the northwest-southeast direction represent Kibarian orogeny while the east-west trend is an indication of Liberian orogeny.

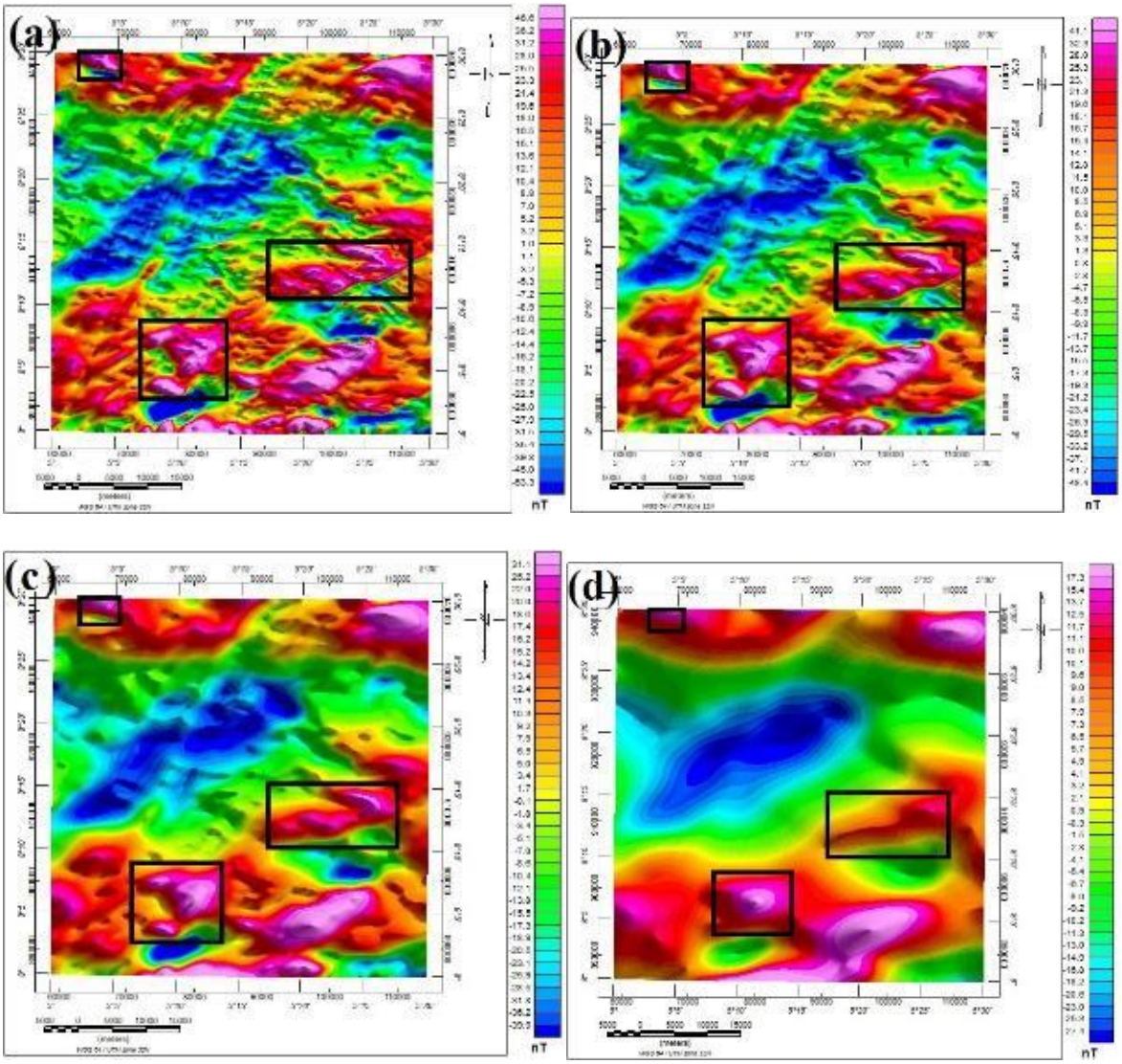

Figure 13 Upward continuation of residual magnetic intensity map to a height of 200 m, 700 m, 1500 m and 3000 m respectively

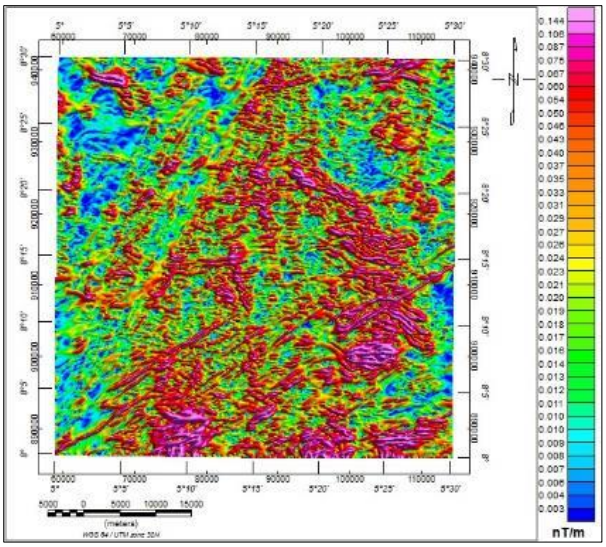

Figure 14 Total horizontal derivative map of the study area

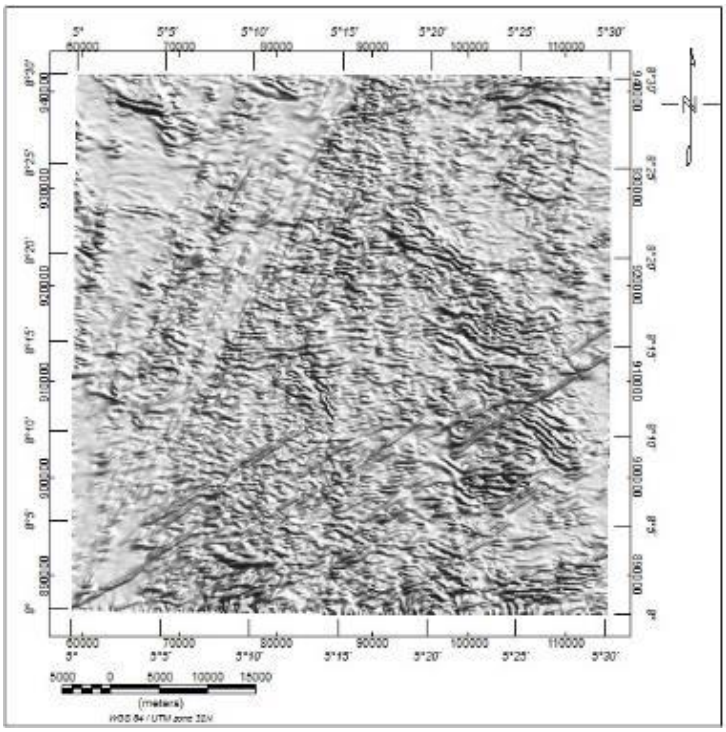

Figure 15 Shaded Relief total horizontal derivative map of the study area

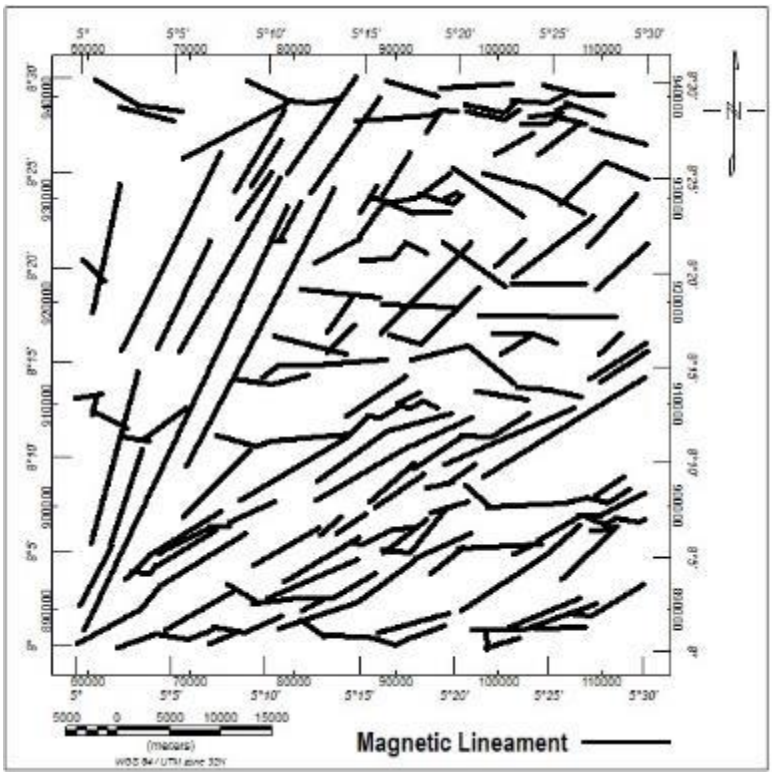

Figure 16 Magnetic Lineaments Map of the study area

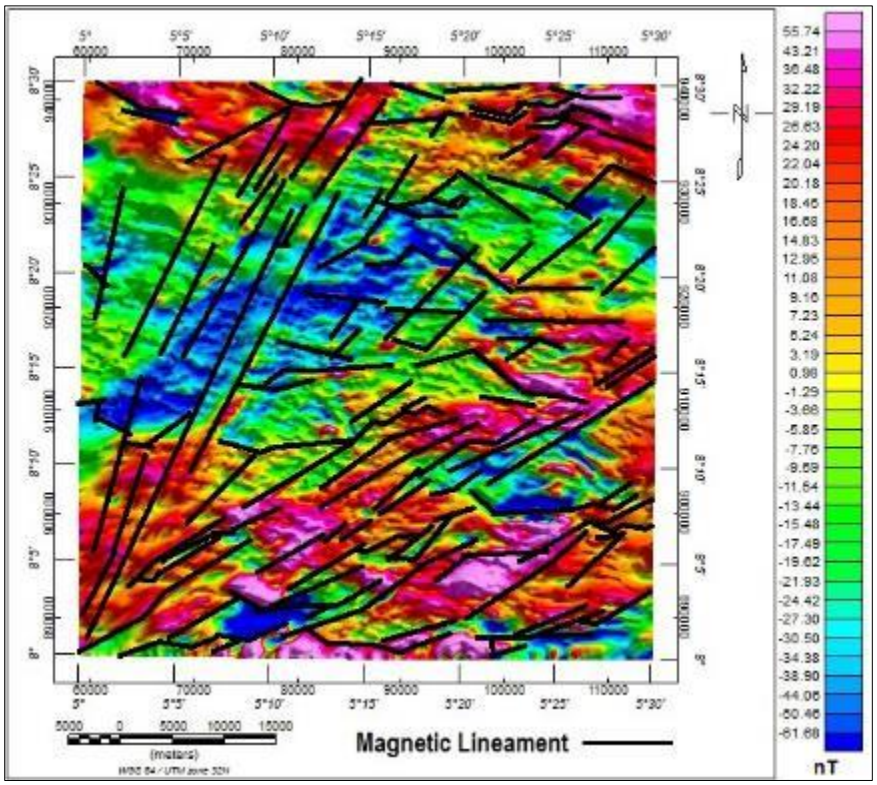

Figure 17 Magnetic lineaments map of the study area

This study further revealed that the Pan African orogeny is the most predominant in the area as shown in Figure 18. The delineated structural features (faults, fractures or lithological boundaries) in the study area ranged between 2 and 20 km in length across the area; as depicted using combined 3D Euler deconvolution, analytical signal magnitude and shaded relief total horizontal derivative maps of the area.

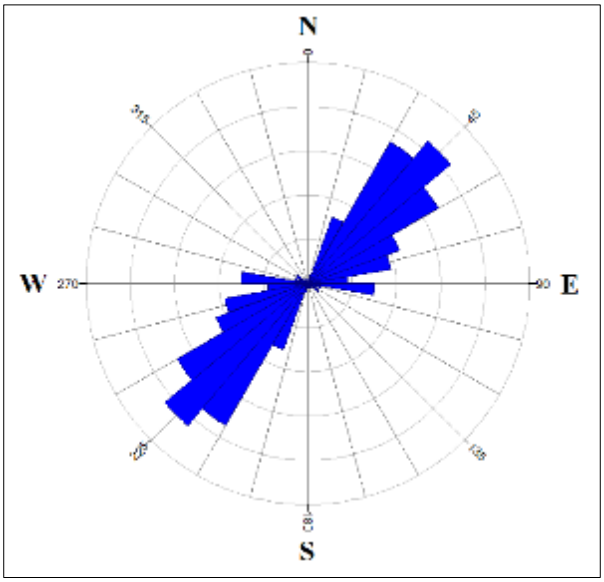

Figure 18 Rose diagram of the inferred magnetic lineaments

7 Conclusion

The possible lithological contact and fault zones in the study area have been successfully delineated by the application of analytical signal magnitude, shaded relief total horizontal derivative, first vertical derivative and 3D Euler deconvolution methods. The analysis of the rose diagram produced revealed that the mapped lineaments strike NE-SW, ENE-WSW, E-W, NW-SE, WNW-ESE, NNE-SSW, and NNW-SSE across the area. The NE-SW and NNE-SSW trending faults in the study area showed evidence of stress history related to Ifewara faults. This is an indication of possible future earthquake occurrence in the area. The identified structures in the study area were depicted to trend majorly in the NE-SW direction suggesting the predominance of the Pan African Orogeny. The depth to magnetic sources as delineated by Euler deconvolution, spectral analysis and source parameter imaging ranged from 118 m to 327 m, 103 m to 460 m and 81 m to 402 m respectively. These values reveal possible depth estimation to the basement in the study area.

Compliance with ethical standards

Acknowledgments

The authors are grateful to the Nigerian Geological Survey Agency for making aeromagnetic data available at low cost.

Disclosure of conflict of interest

No conflict of interest was reported by any of the authors.

References

[1] Maxwell AE, Von Herzen RP, Hsu KJ, Andrews JE, Saito T, Percival SF Deep sea drilling in the South Atlantic. Science. 1970; 168: 1047–1059.

[2] Udensi EE, Osazuwa IB, Daniyan MA The Origin and Tectonic Evolution of the Nupe Basin Nigeria from Aeromagnetic Study. Zuma Journal of Pure and Applied Sciences. 2003; 5: 170-178.

[3] Oluwafemi JO, Ofuyatan OM, Ede AN, Oyebisi SO, Akinwumi II Review of Earthquakes in Nigeria: An Understudied Area. International Journal of Civil Engineering and Technology. 2018; 9: 1023–1033.

[4] Adepelumi AA, Ako BD, Ajayi TR, Olorunfemi AO, Awoyemi MO, Falebita DE Integrated geophysical studies of the Ifewara transcurrent fault system, Nigeria. Journal of African Earth Science. 2008; 52: 161–166.

[5] Awoyemi MO, Ajama OD, Hammed OS, Arogundade AB, Falade SC Geophysical mapping of buried faults in parts of Bida Basin, North Central Nigeria. European Association of Geoscientists & Engineers. Geophysical Prospecting. 2017; 1–15.

[6] Anifowose AYB, Oladapo MI, Akpan OU, Ologun CO, Adeoye-Oladapo OO, Tsebeje SY, Yakubu TA Systematic multi-technique mapping of the southern flank of Iwaraja fault, Nigeria. Journal of Applied Science and Technology. 2010; 15: 70–76.

[7] Affaton P, Rahaman MA, Trompette R, Sougy J The Dahomeyide orogen: tectonothermal evolution and relations with the Volta basin. In: Dallmeyer RD, Lacorche JP (eds) The West African orogens and circum-Atlantic correlatives. Springer-Verlag, Berlin. 1991; 107–122.

[8] Truswell JF, Cope RN The geology of parts of Niger and Zaria provinces, northern Nigeria: Geological Survey of Nigeria. Bull. no. 29. 1963.

[9] Obaje NG Geology and mineral resources of Nigeria. Springer, Dordrecht Heidelberg London New York. 2009; 221 p.

[10] Rahaman MA Recent advances in the study of the basement complex of Nigeria. Symposium on the geology of Nigeria. Obafemi Awolowo University, Nigeria. 1988

[11] Dada SS Proterozoic evolution of Nigeria. In: Oshi O. (ed) The basement complex of Nigeria and its mineral resources. Akin Jinad & Co, Ibadan. 2006; Pp 29–44.

[12] Olade MA, Elueze AA Petrochemistry of the Ilesa amphibolites and Precambrian crustal evolution in the Pan-African domain of SW Nigeria. Precambrian Research. 1979; 8: 303–318.

[13] Obaje NG Geology and Mineral Resources of Nigeria, Lecture Notes in Earth Sciences 120. Springer-Verlag, Berlin. doi:10.1007/978-3-540-92685-6, 2009.

[14] MacLeod IN, Jones K, Dai TF 3-D analytic signal in the interpretation of total magnetic field data at low magnetic latitudes. Exploration Geophysics. 1993; 24: 679–688.

[15] Jeng Y, Lee YL, Chen CY, Lin MJ Integrated Signal Enhancements in Magnetic Investigation in Archaeology. Journal of Applied Geophysics. 2003; 53: 31–48.

[16] Reid AB, Allsop JM, Granser H, Millet AJ, Somerton IW Magnetic interpretation in three dimensions using Euler deconvolution. Geophysics 1990; 55: 80–91.

[17] Thompson DT EULDPH: a new technique for making computer assisted depth estimates from magnetic data. Geophysics 1982; 47: 31–37

[18] Lee YW Statistical theory of communication. Wiley, New York. 1960; Pp 1-75.

[19] Thurston JB, Smith RS Automatic conversion of magnetic data to depth, dip, and susceptibility contrast using the SPI (TM) method. Geophysics. 1997; 62: 807-813.

[20] Thurston JB, Guillon, Smith JC RS Model-independent depth estimation with the SPI™ method: SEG Expand Abstracts 1999; 8: 403-406.

[21] Smith RS, Thurston JB, Dai T, MacLeod IN iSPITM- the improved source parameter imaging method. Geophysical Prospecting. 1998; 46: 141-151.

[22] Nabighian MN, Ander R, Grauch VJS, Hansen RO, LaFehr T, Li Y, Pearson WC, Pierce JW, Phillips JD, Ruder ME The historical development of the gravity method in exploration: Geophysics. 2005; 70: 63-89.

[23] Spector A, Grant FS Statistical Models for interpreting aeromagnetic data. Geophysics. 1970; 35: 293-302.

[24] Bhattacharyya BK Continuous spectrum of the total magnetic field anomaly due to a rectangle prismatic body. Geophysics. 1966; 31: 97-121.

[25] Mishra DC, Naidu PS Two-dimensional power spectral analysis of aeromagnetic fields. Geophysics Prospecting. 1974; 22: 345-353.

[26] Blakely RJ Potential theory in gravity and magnetic applications. Cambridge, UK: Cambridge University Press. 1996; 441 p.

[27] Emberga TT, Timothy C Spectral Re-evaluation of the magnetic basement depth over Yola arm of Upper Benue trough Nigeria using aeromagnetic data. Standard Scientific Research and Essays. 2014; 12: 364-373.